

# Subdiffraction incoherent optical imaging via spatial-mode demultiplexing: semiclassical treatment

Mankei Tsang<sup>1,2,\*</sup>

<sup>1</sup>Department of Electrical and Computer Engineering, National University of Singapore, 4 Engineering Drive 3, Singapore 117583

<sup>2</sup>Department of Physics, National University of Singapore, 2 Science Drive 3, Singapore 117551

\*mankei@nus.edu.sg

## ABSTRACT

I present a semiclassical analysis of a recently proposed spatial-mode demultiplexing (SPADE) scheme for far-field incoherent imaging [M. Tsang, New J. Phys. **19**, 023054 (2017)]. Using only basic concepts in statistical optics, I derive the errors of SPADE in estimating the moments of an arbitrary subdiffraction object. The result proves that SPADE can be far superior to direct imaging for general subdiffraction imaging.

## Introduction

Recent breakthroughs suggest that far-field methods can substantially improve subdiffraction incoherent imaging<sup>1–17</sup>. In particular, Ref. 17 proposes a spatial-mode demultiplexing (SPADE) scheme that can enhance the estimation of moments of an arbitrary subdiffraction object. Although the predicted enhancements are promising for applications in both astronomy and fluorescence microscopy, the theory relies on a quantum formalism that may be difficult to comprehend for researchers in those fields. Here I introduce a semiclassical treatment that reproduces most of the results, assuming only that the readers are familiar with the mutual coherence function and Poisson statistics on the level of Goodman's textbooks<sup>18,19</sup>. The treatment incorporates diffraction, photon shot noise, and—most importantly—coherent optical processing, which enables the enhancements proposed by Refs. 1–17. I also derive the SPADE errors without an approximation used in Ref. 17, thus proving more rigorously the superiority of SPADE over direct imaging.

## Methods

### Statistical optics

Consider the paraxial theory of quasi-monochromatic scalar waves and a spatially incoherent object distribution<sup>18,19</sup>. On the image plane of a diffraction-limited imaging system (depicted in Fig. 1), the mutual coherence function, also called the mutual intensity, can be expressed as<sup>18,19</sup>

$$\Gamma(\mathbf{r}, \mathbf{r}' | \theta) = N \int d^2\mathbf{R} \psi(\mathbf{r} - \mathbf{R}) \psi^*(\mathbf{r}' - \mathbf{R}) F(\mathbf{R} | \theta), \quad (1)$$

where  $F(\mathbf{R} | \theta)$  is the object intensity distribution,  $\mathbf{R} = (X, Y)$  is the two-dimensional object-plane position vector,  $\theta$  is a vector of unknown parameters to be estimated,  $\psi(\mathbf{r})$  is the field point-spread function (PSF), and  $\mathbf{r} = (x, y)$  and  $\mathbf{r}'$  are image-plane position vectors. For convenience, the image-plane coordinates are normalized with respect to the magnification factor, and all the position coordinates are also normalized with respect to the PSF width, such that they are dimensionless and the PSF width is 1 in this dimensionless unit. Assume also the normalization conditions given by

$$\int d^2\mathbf{r} |\psi(\mathbf{r})|^2 = 1, \quad \int d^2\mathbf{R} F(\mathbf{R} | \theta) = 1, \quad (2)$$

and define

$$N = \int d^2\mathbf{r} \Gamma(\mathbf{r}, \mathbf{r} | \theta) \quad (3)$$

as the expected total energy over a given observation time. The expected intensity distribution on the image plane becomes

$$\Gamma(\mathbf{r}, \mathbf{r}|\theta) = Nf(\mathbf{r}|\theta), \quad f(\mathbf{r}|\theta) \equiv \int d^2\mathbf{R} |\psi(\mathbf{r} - \mathbf{R})|^2 F(\mathbf{R}|\theta), \quad (4)$$

which is a basic result in statistical optics.

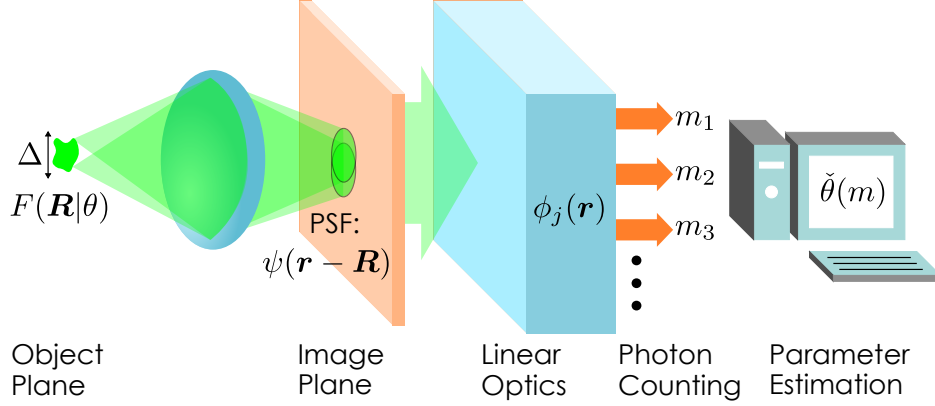


**Figure 1.** A far-field optical imaging system with additional optical processing after the image plane. See the main text for the definitions of the expressions.

Instead of intensity measurement on the image plane, consider the use of further passive linear optics to process the field, as shown in Fig. 1. The expected energy in each output channel can be expressed as

$$\bar{m}_j(\theta) = \int d^2\mathbf{r} \int d^2\mathbf{r}' \phi_j(\mathbf{r}) \phi_j^*(\mathbf{r}') \Gamma(\mathbf{r}, \mathbf{r}'|\theta) = N \int d^2\mathbf{R} \left| \int d^2\mathbf{r} \phi_j(\mathbf{r}) \psi(\mathbf{r} - \mathbf{R}) \right|^2 F(\mathbf{R}|\theta). \quad (5)$$

If the optics is lossless, energy conservation ( $\sum_j \bar{m}_j = N$ ) implies that the impulse-response function  $\phi_j(\mathbf{r})$  is unitary, satisfying

$$\sum_j \phi_j(\mathbf{r}) \phi_j^*(\mathbf{r}') = \delta^2(\mathbf{r} - \mathbf{r}'), \quad \int d^2\mathbf{r} \phi_j(\mathbf{r}) \phi_k^*(\mathbf{r}) = \delta_{jk}. \quad (6)$$

In other words,  $\{\phi_j(\mathbf{r})\}$  is an orthonormal basis, and any linear optics can be regarded as mode demultiplexing<sup>3,20</sup>. For example, direct imaging, which measures the spatial intensity distribution on the image plane, can be modeled by  $\phi_j(\mathbf{r}) = \sqrt{d^2\mathbf{r}} \delta^2(\mathbf{r}_j - \mathbf{r})$ , where  $\mathbf{r}_j$  is the position of each pixel with infinitesimal area  $d^2\mathbf{r}$ , such that  $\bar{m}_j(\theta) = Nd^2\mathbf{r} f(\mathbf{r}_j|\theta)$ . Optical losses can be modeled by introducing auxiliary inaccessible channels to the lossless model<sup>3</sup>.

For weak incoherent sources, such as astronomical optical sources and microscopic fluorophores, bunching or antibunching is negligible, and it is standard to assume a Poisson model for the photon counts  $m = (m_1, m_2, \dots)$  at the output channels<sup>3,19,21–24</sup>. Assuming that each  $\bar{m}_j(\theta)$  is in the unit of photon number, the probability distribution is

$$P(m|\theta) = \prod_j \exp[-\bar{m}_j(\theta)] \frac{[\bar{m}_j(\theta)]^{m_j}}{m_j!}. \quad (7)$$

The quantum formalism arrives at the same conclusion by assuming that the average photon number per mode is much smaller than 1 and the photon count for each channel is integrated over multiple temporal modes<sup>1,17</sup>. The most important statistics here are the mean

$$\mathbb{E}(m_j) = \bar{m}_j(\theta) \quad (8)$$

and the covariance matrix

$$\mathbb{E}(m_j m_k) - \mathbb{E}(m_j) \mathbb{E}(m_k) = \bar{m}_j(\theta) \delta_{jk}, \quad (9)$$

where  $\mathbb{E}(g) \equiv \sum_m g(m) P(m|\theta)$  is the expectation.

## Cramér-Rao bounds

To investigate the limits of imaging, a useful and now standard tool is the Cramér-Rao bound (CRB) on the mean-square error of any estimator  $\hat{\theta}(m)$  that satisfies the unbiased condition  $\mathbb{E}(\hat{\theta}) = \theta$ <sup>21,24–26</sup>:

$$\text{MSE}_\mu(\theta) \equiv \mathbb{E}(\hat{\theta}_\mu - \theta_\mu)^2 \geq \text{CRB}_{\mu\mu}(\theta), \quad \text{CRB}(\theta) \equiv J^{-1}(\theta), \quad (10)$$

where

$$J_{\mu\nu}(\theta) \equiv \sum_m \frac{1}{P(m|\theta)} \frac{\partial P(m|\theta)}{\partial \theta_\mu} \frac{\partial P(m|\theta)}{\partial \theta_\nu} \quad (11)$$

is called the Fisher information matrix. For the Poisson model, it is given by

$$J_{\mu\nu}(\theta) = \sum_j \frac{1}{\bar{m}_j(\theta)} \frac{\partial \bar{m}_j(\theta)}{\partial \theta_\mu} \frac{\partial \bar{m}_j(\theta)}{\partial \theta_\nu}. \quad (12)$$

For example, the information for ideal direct imaging is

$$J_{\mu\nu}^{(\text{direct})}(\theta) = N \int d^2\mathbf{r} \frac{1}{f(\mathbf{r}|\theta)} \frac{\partial f(\mathbf{r}|\theta)}{\partial \theta_\mu} \frac{\partial f(\mathbf{r}|\theta)}{\partial \theta_\nu}, \quad (13)$$

assuming for simplicity that  $N$  is given.

An intuitive way of understanding Eq. (12) is to regard it as a signal-to-noise ratio: each derivative  $\partial \bar{m}_j(\theta)/\partial \theta_\mu$  measures the sensitivity of a channel to a parameter, and the denominator  $\bar{m}_j(\theta)$ —equal to the Poisson variance—indicates the noise level. The form of Eq. (12) hence suggests that any parameter-insensitive background in  $\bar{m}_j(\theta)$  should be minimized.

A more general limit valid for any biased or unbiased estimator can be expressed in terms of the Bayesian CRB (BCRB) as<sup>5,25,27,28</sup>

$$\int d\theta p(\theta) \text{MSE}_\mu(\theta) \geq \text{BCRB}_{\mu\mu}, \quad \text{BCRB} \equiv (\bar{J} + j)^{-1}, \quad (14)$$

where  $p(\theta)$  is a prior probability density that vanishes on the boundary of its domain,

$$\bar{J} \equiv \int d\theta p(\theta) J(\theta) \quad (15)$$

is the average Fisher information, and

$$j_{\mu\nu} \equiv \int d\theta \frac{1}{p(\theta)} \frac{\partial p(\theta)}{\partial \theta_\mu} \frac{\partial p(\theta)}{\partial \theta_\nu} \quad (16)$$

is the prior information. Other Bayesian bounds for more general priors can be found in Ref. 29.

For minimax estimation<sup>5,28</sup>, the quantity of interest is the worst-case error  $\sup_\theta \text{MSE}_\mu(\theta)$ . Since

$$\sup_\theta \text{MSE}_\mu(\theta) \geq \int d\theta p(\theta) \text{MSE}_\mu(\theta) \quad (17)$$

for any  $p(\theta)$ ,  $p(\theta)$  can be chosen to tighten the BCRB on the worst-case error<sup>5,28</sup>.

## Moment estimation by direct imaging

Define the object moments as

$$\theta_\mu = \int d^2\mathbf{r} \mathbf{r} \mathbf{r}^\mu F(\mathbf{r}|\theta), \quad \boldsymbol{\mu} = (\mu_X, \mu_Y) \in \mathbb{N}^2, \quad (18)$$

where  $\mathbb{N} \equiv \{0, 1, 2, \dots\}$  and I have introduced the notation

$$\mathbf{r}^\mu \equiv X^{\mu_X} Y^{\mu_Y}. \quad (19)$$

The normalization condition given by Eq. (2) mandates that  $\theta_{00} = 1$ , but all the other moments are assumed to be unknown. Assuming the Gaussian PSF

$$\psi(\mathbf{r}) = \frac{1}{\sqrt{2\pi}} \exp\left(-\frac{|\mathbf{r}|^2}{4}\right), \quad (20)$$

as is common in fluorescence microscopy<sup>24,26</sup>, and expanding the  $|\psi(\mathbf{r} - \mathbf{R})|^2$  in Eq. (4) in a Taylor series, it can be shown that

$$f(\mathbf{r}|\theta) = |\psi(\mathbf{r})|^2 \sum_{\boldsymbol{\mu} \in \mathbb{N}^2} \frac{\text{He}_{\boldsymbol{\mu}}(\mathbf{r})}{\boldsymbol{\mu}!} \theta_{\boldsymbol{\mu}}, \quad (21)$$

where I have introduced the shorthands

$$\text{He}_{\boldsymbol{\mu}}(\mathbf{r}) \equiv \text{He}_{\mu_x}(x) \text{He}_{\mu_y}(y), \quad \boldsymbol{\mu}! \equiv \mu_x! \mu_y!, \quad (22)$$

and  $\text{He}_{\mu}(x)$  is the Hermite polynomial<sup>30,31</sup>.

Define the object width as the minimum  $\Delta$  such that

$$F(\mathbf{R}|\theta) = 0 \text{ for } |\mathbf{R}| > \frac{\Delta}{2}, \quad (23)$$

and define the scenario where  $\Delta$  is much smaller than the PSF width, viz.,

$$\Delta \ll 1, \quad (24)$$

as the subdiffraction regime. Substituting Eq. (21) into Eq. (13), rewriting the denominator as  $f(\mathbf{r}|\theta) = |\psi(\mathbf{r})|^2 [1 + O(\Delta)]$ , and applying the orthogonality relations of the Hermite polynomials given by  $\int_{-\infty}^{\infty} dx \exp(-x^2/2) \text{He}_{\mu}(x) \text{He}_{\nu}(x) = \sqrt{2\pi} \mu! \delta_{\mu\nu}$ <sup>30,31</sup>, Ref. 17 shows that

$$J_{\boldsymbol{\mu}\boldsymbol{\nu}}^{(\text{direct})}(\theta) = \frac{N}{\boldsymbol{\mu}!} [\delta_{\boldsymbol{\mu}\boldsymbol{\nu}} + O(\Delta)], \quad \text{CRB}_{\boldsymbol{\mu}\boldsymbol{\mu}}^{(\text{direct})}(\theta) = \frac{\boldsymbol{\mu}!}{N} [1 + O(\Delta)]. \quad (25)$$

The almost constant Fisher information means that  $\tilde{J}_{\boldsymbol{\mu}\boldsymbol{\nu}}^{(\text{direct})} \approx (N/\boldsymbol{\mu}!) \delta_{\boldsymbol{\mu}\boldsymbol{\nu}}$  for any prior in the subdiffraction regime. This implies that, for any reasonable prior that gives a finite prior information  $j$ , a large enough  $N$  can make  $\tilde{J}^{(\text{direct})}$  much larger than  $j$  in Eq. (14), leading to

$$\text{BCRB}_{\boldsymbol{\mu}\boldsymbol{\mu}}^{(\text{direct})} \approx \frac{\boldsymbol{\mu}!}{N}. \quad (26)$$

Note that the CRB and the BCRB here are close, unlike those in the problem of two-point separation estimation<sup>5</sup>, where the Fisher information vanishes at a point in the parameter space and the choice of prior for the worst-case error bound becomes nontrivial<sup>5,28</sup>.

The next section proves that SPADE can achieve much lower errors.

## Results

### Moment estimation by TEM scheme

Consider the transverse-electromagnetic (TEM) basis given by  $\{\phi_{\mathbf{q}}(\mathbf{r}); \mathbf{q} = (q_x, q_y) \in \mathbb{N}^2\}$ , where

$$\phi_{\mathbf{q}}(\mathbf{r}) = \frac{\text{He}_{\mathbf{q}}(\mathbf{r})}{\sqrt{2\pi} \mathbf{q}!} \exp\left(-\frac{|\mathbf{r}|^2}{4}\right). \quad (27)$$

Some low-order mode functions are plotted in Fig. 2. Using the generating function  $\exp(xz - z^2/2) = \sum_{q=0}^{\infty} \text{He}_q(x) z^q / q!$ <sup>30,31</sup>, it can be shown that

$$\psi(\mathbf{r} - \mathbf{R}) = \exp\left(-\frac{|\mathbf{R}|^2}{8}\right) \sum_{\mathbf{q} \in \mathbb{N}^2} \frac{\mathbf{R}^{\mathbf{q}}}{2^{|\mathbf{q}|_1} \sqrt{\mathbf{q}!}} \phi_{\mathbf{q}}(\mathbf{r}), \quad (28)$$

where I have defined

$$|\mathbf{q}|_1 \equiv q_x + q_y. \quad (29)$$

The expected photon count given by Eq. (5) in a TEM mode becomes<sup>14,17</sup>

$$\bar{m}_{\mathbf{q}} = N^{(\text{TEM})} C(\mathbf{q}, \mathbf{q}) \Theta_{2\mathbf{q}}, \quad C(\mathbf{q}, \mathbf{q}') \equiv \frac{1}{2^{|\mathbf{q}+\mathbf{q}'|_1} \sqrt{\mathbf{q}! \mathbf{q}'!}}, \quad \Theta_{\boldsymbol{\mu}} \equiv \int d^2 \mathbf{R} \mathbf{R}^{\boldsymbol{\mu}} \exp\left(-\frac{|\mathbf{R}|^2}{4}\right) F(\mathbf{R}|\theta), \quad (30)$$

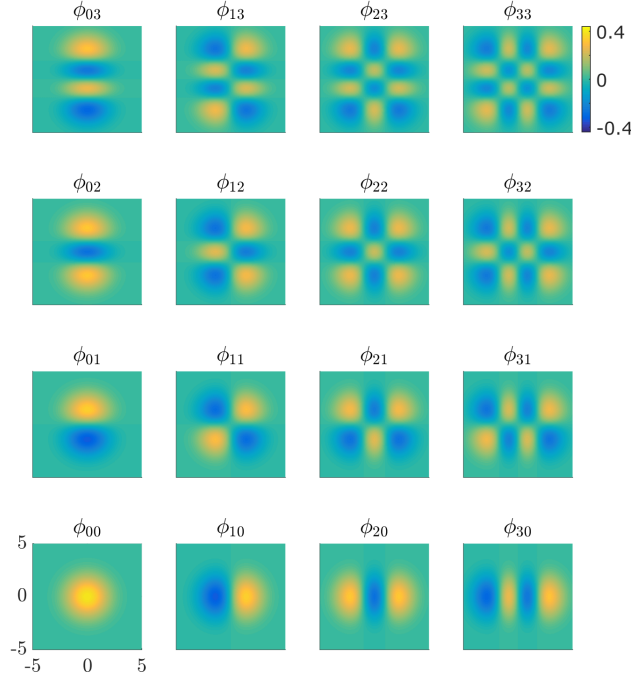


**Figure 2.** Plots of some low-order TEM mode functions given by Eq. (27).

where the superscript on  $N^{(\text{TEM})}$  emphasizes that the TEM scheme may take only a fraction of the available photons in practice.

To proceed, Ref. 17 assumes simply  $\Theta_{\mu} \approx \theta_{\mu}$  for subdiffraction objects, without quantifying the systematic errors that may arise from such an approximation. Here I consider the exact relation given by

$$\begin{aligned} \theta_{\mu} &= \int d^2 \mathbf{R} \mathbf{R} \mathbf{R}^{\mu} \exp\left(\frac{|\mathbf{R}|^2}{4}\right) \exp\left(-\frac{|\mathbf{R}|^2}{4}\right) F(\mathbf{R}|\theta) = \int d^2 \mathbf{R} \mathbf{R} \mathbf{R}^{\mu} \left[ \sum_{\mathbf{p} \in \mathbb{N}^2} C(\mathbf{p}, \mathbf{p}) \mathbf{R}^{2\mathbf{p}} \right] \exp\left(-\frac{|\mathbf{R}|^2}{4}\right) F(\mathbf{R}|\theta) \\ &= \sum_{\mathbf{p} \in \mathbb{N}^2} C(\mathbf{p}, \mathbf{p}) \Theta_{\mu+2\mathbf{p}}. \end{aligned} \quad (31)$$

This linear relation implies that an unbiased estimator of  $\theta_{\mu}$  can be constructed from unbiased estimators of  $\Theta_{\mu+2\mathbf{p}}$  as

$$\check{\theta}_{\mu} = \sum_{\mathbf{p} \in \mathbb{N}^2} C(\mathbf{p}, \mathbf{p}) \check{\Theta}_{\mu+2\mathbf{p}}. \quad (32)$$

For example, given the photon counts  $\{m_{\mathbf{q}}\}$  from the TEM scheme, an unbiased estimator of the moment  $\theta_{2\mathbf{q}}$  is

$$\check{\theta}_{2\mathbf{q}} = \sum_{\mathbf{p} \in \mathbb{N}^2} C(\mathbf{p}, \mathbf{p}) \check{\Theta}_{2\mathbf{q}+2\mathbf{p}}, \quad \check{\Theta}_{2\mathbf{q}+2\mathbf{p}} = \frac{m_{\mathbf{q}+\mathbf{p}}}{N^{(\text{TEM})} C(\mathbf{q} + \mathbf{p}, \mathbf{q} + \mathbf{p})}. \quad (33)$$

The unbiased conditions  $\mathbb{E}(\check{\Theta}_{2\mathbf{q}+2\mathbf{p}}) = \Theta_{2\mathbf{q}+2\mathbf{p}}$  and  $\mathbb{E}(\check{\theta}_{2\mathbf{q}}) = \theta_{2\mathbf{q}}$  can be derived from Eqs. (30) and (31). The mean-square error becomes

$$\text{MSE}_{2\mathbf{q}} = \mathbb{V}(\check{\theta}_{2\mathbf{q}}) = \sum_{\mathbf{p} \in \mathbb{N}^2} C^2(\mathbf{p}, \mathbf{p}) \mathbb{V}(\check{\Theta}_{2\mathbf{q}+2\mathbf{p}}), \quad \mathbb{V}(\check{\Theta}_{2\mathbf{q}+2\mathbf{p}}) = \frac{\Theta_{2\mathbf{q}+2\mathbf{p}}}{N^{(\text{TEM})} C(\mathbf{q} + \mathbf{p}, \mathbf{q} + \mathbf{p})}, \quad (34)$$

where  $\mathbb{V}(g) \equiv \mathbb{E}(g^2) - \mathbb{E}^2(g)$  is the variance. With

$$|\Theta_{\mu}| \leq \left(\frac{\Delta}{2}\right)^{|\mu|_1}, \quad (35)$$

the convergence of Eq. (34) can be proved using the ratio test<sup>32</sup>. Equation (35) also means that, in the subdiffraction regime, Eq. (34) is dominated by the leading-order term

$$\mathbb{V}(\check{\Theta}_{2\mathbf{q}}) = \frac{\Theta_{2\mathbf{q}}}{N^{(\text{TEM})}C(\mathbf{q}, \mathbf{q})} \leq \frac{\mathbf{q}!\Delta^{2|\mathbf{q}|_1}}{N^{(\text{TEM})}}. \quad (36)$$

In other words,

$$\text{MSE}_{2\mathbf{q}} = \mathbb{V}(\check{\Theta}_{2\mathbf{q}}) + \frac{O(\Delta^{2|\mathbf{q}|_1+2})}{N^{(\text{TEM})}} = \frac{O(\Delta^{2|\mathbf{q}|_1})}{N^{(\text{TEM})}}. \quad (37)$$

Compared with the CRB for direct imaging given by Eq. (25), which does not depend on  $\Delta$  to the leading order, the errors of the TEM scheme can be significantly smaller when  $\Delta \ll 1$ . An intuitive explanation is as follows: In the subdiffraction regime, the noise in direct imaging mostly comes from the TEM<sub>00</sub> mode, which acts as a background. The TEM scheme, on the other hand, can separate all the lower-order modes—including the TEM<sub>00</sub> mode—from each output. As a result, the expected photon count given by Eq. (30) contains no parameter-insensitive background, and the Poisson noise is reduced without compromising the sensitivity.

In practice, only a finite number of channels can be measured. Consider the finite-channel estimator

$$\check{\Theta}'_{2\mathbf{q}} = \sum_{\mathbf{p}=(0,0)}^{\mathbf{p}'} C(\mathbf{p}, \mathbf{p}) \check{\Theta}_{2\mathbf{q}+2\mathbf{p}}, \quad (38)$$

which uses only modes with orders from  $\mathbf{q}$  to  $\mathbf{q} + \mathbf{p}'$  and now has a bias given by

$$\mathbb{E}(\check{\Theta}'_{2\mathbf{q}}) - \Theta_{2\mathbf{q}} = O\left(\Delta^{2|\mathbf{q}|_1+2|\mathbf{p}'|_1+2}\right). \quad (39)$$

The error becomes

$$\text{MSE}'_{2\mathbf{q}} = \mathbb{V}(\check{\Theta}'_{2\mathbf{q}}) + [\mathbb{E}(\check{\Theta}'_{2\mathbf{q}}) - \Theta_{2\mathbf{q}}]^2 = \frac{O(\Delta^{2|\mathbf{q}|_1})}{N^{(\text{TEM})}} + O\left(\Delta^{4|\mathbf{q}|_1+4|\mathbf{p}'|_1+4}\right). \quad (40)$$

Unlike the estimator variance, the error due to the bias here does not scale with the photon number, although its order with respect to  $\Delta$  is much higher and depends on  $|\mathbf{p}'|_1$ . This means that the number of measured modes can be chosen to reduce the bias and make the total error acceptable. For example, the numerical demonstration in Ref. 17 assumes simply  $\check{\Theta}'_{2\mathbf{q}} = \check{\Theta}_{2\mathbf{q}}$  with  $|\mathbf{p}'|_1 = 0$  but still obtains negligible biases.

### iTEM1 and iTEM4 schemes

The interferometric TEM (iTEM) measurement proposed in Ref. 17 assumes the following pair of projections:

$$\phi_+^{(\mathbf{q}, \mathbf{q}')}(\mathbf{r}) = \frac{1}{\sqrt{2}} [\phi_{\mathbf{q}}(\mathbf{r}) + \phi_{\mathbf{q}'}(\mathbf{r})], \quad \phi_-^{(\mathbf{q}, \mathbf{q}')}(\mathbf{r}) = \frac{1}{\sqrt{2}} [\phi_{\mathbf{q}}(\mathbf{r}) - \phi_{\mathbf{q}'}(\mathbf{r})], \quad (41)$$

which result from the interference of two TEM modes. The expected photon counts are

$$\bar{m}_+^{(\mathbf{q}, \mathbf{q}')} = N [\beta(\mathbf{q}, \mathbf{q}') + C(\mathbf{q}, \mathbf{q}')\Theta_{\mathbf{q}+\mathbf{q}'}], \quad \bar{m}_-^{(\mathbf{q}, \mathbf{q}')} = N [\beta(\mathbf{q}, \mathbf{q}') - C(\mathbf{q}, \mathbf{q}')\Theta_{\mathbf{q}+\mathbf{q}'}], \quad (42)$$

$$\beta(\mathbf{q}, \mathbf{q}') \equiv \frac{1}{2} [C(\mathbf{q}, \mathbf{q})\Theta_{2\mathbf{q}} + C(\mathbf{q}', \mathbf{q}')\Theta_{2\mathbf{q}'}]. \quad (43)$$

Given the two photon counts  $m_+^{(\mathbf{q}, \mathbf{q}')}$  and  $m_-^{(\mathbf{q}, \mathbf{q}')}$ , an unbiased estimator of  $\Theta_{\mathbf{q}+\mathbf{q}'}$  can be constructed as

$$\check{\Theta}_{\mathbf{q}+\mathbf{q}'} = \frac{m_+^{(\mathbf{q}, \mathbf{q}')} - m_-^{(\mathbf{q}, \mathbf{q}')}}{2NC(\mathbf{q}, \mathbf{q}')}, \quad (44)$$

$$\mathbb{V}(\check{\Theta}_{\mathbf{q}+\mathbf{q}'}) = \frac{\beta(\mathbf{q}, \mathbf{q}')}{2NC^2(\mathbf{q}, \mathbf{q}')} = \frac{O(\Delta^{2\min(|\mathbf{q}|_1, |\mathbf{q}'|_1)})}{N}. \quad (45)$$

Multiple iTEM measurements can be applied simultaneously as long as the projections are orthogonal; Ref. 17 proposes 7 bases of orthogonal modes, named TEM and iTEM1–iTEM6 schemes, that can be used for the estimation of all  $\Theta_{\boldsymbol{\mu}}$ .

The iTEM1 scheme consists of projections with

$$q_x \in \{0, 2, 4, \dots\}, \quad q_y \in \{0, 1, 2, \dots\}, \quad \mathbf{q}' = \mathbf{q} + (1, 0), \quad (46)$$

such that it is sensitive to  $\Theta_{\boldsymbol{\mu}}$  with

$$\mu_X \in \{1, 5, 9, \dots\}, \quad \mu_Y \in \{0, 2, 4, \dots\}, \quad (47)$$

while the iTEM4 scheme consists of projections with

$$q_x \in \{1, 3, 5, \dots\}, \quad q_y \in \{0, 1, 2, \dots\}, \quad \mathbf{q}' = \mathbf{q} + (1, 0), \quad (48)$$

such that it is sensitive to  $\Theta_{\boldsymbol{\mu}}$  with

$$\mu_X \in \{3, 7, 11, \dots\}, \quad \mu_Y \in \{0, 2, 4, \dots\}. \quad (49)$$

The two schemes together offer sensitivity to any  $\Theta_{\boldsymbol{\mu}}$  with odd  $\mu_X$  and even  $\mu_Y$ , allowing an unbiased estimator of  $\theta_{\boldsymbol{\mu}}$  with odd  $\mu_X$  and even  $\mu_Y$  to be constructed from their outputs according to Eqs. (32) and (44). Assuming that the iTEM1 scheme receives  $N^{(\text{iTEM1})}$  photons on average and the iTEM4 scheme also receives  $O(N^{(\text{iTEM1})})$  photons, Eq. (45) leads to

$$\mathbb{V}(\check{\Theta}_{\boldsymbol{\mu}}) = \frac{O(\Delta^{|\boldsymbol{\mu}|_1 - 1})}{N^{(\text{iTEM1})}}, \quad (50)$$

and the error becomes

$$\text{MSE}_{\boldsymbol{\mu}} = \mathbb{V}(\check{\Theta}_{\boldsymbol{\mu}}) = \sum_{\mathbf{p} \in \mathbb{N}^2} C^2(\mathbf{p}, \mathbf{p}) \mathbb{V}(\check{\Theta}_{\boldsymbol{\mu} + 2\mathbf{p}}) = \frac{O(\Delta^{|\boldsymbol{\mu}|_1 - 1})}{N^{(\text{iTEM1})}}, \quad (51)$$

which can offer substantial improvements over the direct-imaging CRB given by Eq. (25) for the  $|\boldsymbol{\mu}|_1 > 1$  moments.

With a finite number of channels, the estimator

$$\check{\theta}'_{\boldsymbol{\mu}} = \sum_{\mathbf{p}=(0,0)}^{\mathbf{p}'} C(\mathbf{p}, \mathbf{p}) \check{\Theta}_{\boldsymbol{\mu} + 2\mathbf{p}} \quad (52)$$

has a bias

$$\mathbb{E}(\check{\theta}'_{\boldsymbol{\mu}}) - \theta_{\boldsymbol{\mu}} = O\left(\Delta^{|\boldsymbol{\mu}|_1 + 2|\mathbf{p}'|_1 + 2}\right), \quad (53)$$

and the error becomes

$$\text{MSE}'_{\boldsymbol{\mu}} = \frac{O(\Delta^{|\boldsymbol{\mu}|_1 - 1})}{N^{(\text{iTEM1})}} + O\left(\Delta^{2|\boldsymbol{\mu}|_1 + 4|\mathbf{p}'|_1 + 4}\right). \quad (54)$$

$\mathbf{p}'$  should again be chosen to keep the total error acceptable in practice.

## iTEM2 and iTEM5 schemes

The analysis of the iTEM2 and iTEM5 schemes is identical to that in the previous section, except that the  $x$  and  $y$  dimensions are switched. The iTEM2 scheme consists of projections with

$$q_x \in \{0, 1, 2, \dots\}, \quad q_y \in \{0, 2, 4, \dots\}, \quad \mathbf{q}' = \mathbf{q} + (0, 1), \quad (55)$$

such that it is sensitive to  $\Theta_{\boldsymbol{\mu}}$  with

$$\mu_X \in \{0, 2, 4, \dots\}, \quad \mu_Y \in \{1, 5, 9, \dots\}, \quad (56)$$

while the iTEM5 scheme consists of projections with

$$q_x \in \{0, 1, 2, \dots\}, \quad q_y \in \{1, 3, 5, \dots\}, \quad \mathbf{q}' = \mathbf{q} + (0, 1), \quad (57)$$

such that it is sensitive to  $\Theta_{\boldsymbol{\mu}}$  with

$$\mu_X \in \{0, 2, 4, \dots\}, \quad \mu_Y \in \{3, 7, 11, \dots\}. \quad (58)$$

An unbiased estimator of  $\theta_{\boldsymbol{\mu}}$  with even  $\mu_X$  and odd  $\mu_Y$  can be constructed from the outputs of the two schemes according to Eqs. (32) and (44). Assuming that the iTEM2 scheme receives  $N^{(\text{iTEM2})}$  photons and the iTEM5 scheme also receives  $O(N^{(\text{iTEM2})})$  photons, the estimation errors have the same expressions as Eqs. (51) and (54), with  $N^{(\text{iTEM2})}$  replacing  $N^{(\text{iTEM1})}$ .

### iTEM3 and iTEM6 schemes

The iTEM3 scheme consists of projections with

$$q_x \in \{0, 1, 2, \dots\}, \quad q_y \in \{1, 3, 5, \dots\}, \quad \mathbf{q}' = \mathbf{q} + (1, -1), \quad (59)$$

such that it is sensitive to  $\Theta_{\boldsymbol{\mu}}$  with

$$\mu_x \in \{1, 3, 5, \dots\}, \quad \mu_y \in \{1, 5, 9, \dots\}, \quad (60)$$

while the iTEM6 scheme consists of projections with

$$q_x \in \{0, 1, 2, \dots\}, \quad q_y \in \{2, 4, 6, \dots\}, \quad \mathbf{q}' = \mathbf{q} + (1, -1), \quad (61)$$

such that it is sensitive to  $\Theta_{\boldsymbol{\mu}}$  with

$$\mu_x \in \{1, 3, 5, \dots\}, \quad \mu_y \in \{3, 7, 11, \dots\}. \quad (62)$$

An unbiased estimator of  $\theta_{\boldsymbol{\mu}}$  with odd  $\mu_x$  and odd  $\mu_y$  can be constructed from the outputs of the iTEM3 and iTEM6 schemes according to Eqs. (32) and (44). Assuming that the iTEM3 scheme receives  $N^{(\text{iTEM3})}$  photons on average and the iTEM6 scheme also receives  $O(N^{(\text{iTEM3})})$  photons, Eq. (45) implies

$$\mathbb{V}(\check{\Theta}_{\boldsymbol{\mu}}) = \frac{O(\Delta^{|\boldsymbol{\mu}|_1})}{N^{(\text{iTEM3})}}. \quad (63)$$

The error becomes

$$\text{MSE}_{\boldsymbol{\mu}} = \frac{O(\Delta^{|\boldsymbol{\mu}|_1})}{N^{(\text{iTEM3})}} \quad (64)$$

for the estimator given by Eq. (32), and

$$\text{MSE}'_{\boldsymbol{\mu}} = \frac{O(\Delta^{|\boldsymbol{\mu}|_1})}{N^{(\text{iTEM3})}} + O\left(\Delta^{2|\boldsymbol{\mu}|_1+4|p'|_1+4}\right) \quad (65)$$

for the finite-channel estimator given by Eq. (52).

## Discussion

The semiclassical treatment here complements the quantum approach in Ref. 17 by offering a shortcut to the Poisson photon-counting model for weak incoherent sources, passive linear optics, and photon counting. Besides a new perspective, this work presents a new form of estimators for SPADE and more rigorous expressions for their errors, without resorting to the  $\Theta_{\boldsymbol{\mu}} \approx \theta_{\boldsymbol{\mu}}$  approximation used in Ref. 17 or asymptotic arguments. The resulting errors turn out to be equal to the ones suggested in Ref. 17 in the leading order. The conclusion of Ref. 17 hence remains intact: SPADE can indeed improve upon direct imaging in estimating the second and higher moments of a subdiffraction object.

The linear and unbiased form of the estimators is chosen here on account of its tractability, but nonlinear or biased estimators may perform even better. For example, the maximum-likelihood estimator<sup>25</sup> for this problem is nonlinear and able to combine all the outputs of the different schemes, while more advanced estimators in modern Bayesian or minimax statistics may also help.

Experimental implementations and generalizations for non-Gaussian PSFs are important future directions. For proof-of-concept demonstrations, it should be possible to use the same setups described in Refs. 13–16 to estimate at least the second moments of more general objects. For other PSFs, the theory outlined in Refs. 9, 11 seems promising.

To bring SPADE into practice for fluorescence microscopy and telescoping, efficient demultiplexing for broadband sources is needed. The technical challenge is by no means trivial, but the promise of giant enhancements using only far-field linear optics should motivate further efforts.

## References

1. Tsang, M., Nair, R. & Lu, X.-M. Quantum theory of superresolution for two incoherent optical point sources. *Phys. Rev. X* **6**, 031033 (2016). URL <http://link.aps.org/doi/10.1103/PhysRevX.6.031033>. DOI 10.1103/PhysRevX.6.031033.

2. Nair, R. & Tsang, M. Interferometric superlocalization of two incoherent optical point sources. *Opt. Express* **24**, 3684–3701 (2016). URL <http://www.opticsexpress.org/abstract.cfm?URI=oe-24-4-3684>. DOI 10.1364/OE.24.003684.
3. Tsang, M., Nair, R. & Lu, X.-M. Quantum information for semiclassical optics. In *Proc. SPIE*, vol. 10029 of *Quantum and Nonlinear Optics IV*, 1002903 (2016). URL <http://dx.doi.org/10.1117/12.2245733>. DOI 10.1117/12.2245733.
4. Nair, R. & Tsang, M. Far-Field Superresolution of Thermal Electromagnetic Sources at the Quantum Limit. *Phys. Rev. Lett.* **117**, 190801 (2016). URL <http://link.aps.org/doi/10.1103/PhysRevLett.117.190801>. DOI 10.1103/PhysRevLett.117.190801.
5. Tsang, M. Conservative classical and quantum resolution limits for incoherent imaging. *arXiv:1605.03799 [physics, physics:quant-ph]* (2017). URL <http://arxiv.org/abs/1605.03799>.
6. Ang, S. Z., Nair, R. & Tsang, M. Quantum limit for two-dimensional resolution of two incoherent optical point sources. *Phys. Rev. A* **95**, 063847 (2017). URL <https://link.aps.org/doi/10.1103/PhysRevA.95.063847>. DOI 10.1103/PhysRevA.95.063847.
7. Lu, X.-M., Nair, R. & Tsang, M. Quantum-optimal detection of one-versus-two incoherent sources with arbitrary separation. *arXiv:1609.03025 [quant-ph]* (2016). URL <http://arxiv.org/abs/1609.03025>.
8. Lupo, C. & Pirandola, S. Ultimate Precision Bound of Quantum and Subwavelength Imaging. *Phys. Rev. Lett.* **117**, 190802 (2016). URL <http://link.aps.org/doi/10.1103/PhysRevLett.117.190802>. DOI 10.1103/PhysRevLett.117.190802.
9. Rehacek, J., Pařr, M., Stoklasa, B., Hradil, Z. & Sánchez-Soto, L. L. Optimal measurements for resolution beyond the Rayleigh limit. *Opt. Lett.* **42**, 231–234 (2017). URL <http://www.osapublishing.org/abstract.cfm?uri=ol-42-2-231>. DOI 10.1364/OL.42.000231.
10. Krovi, H., Guha, S. & Shapiro, J. H. Attaining the quantum limit of passive imaging. *arXiv:1609.00684 [physics, physics:quant-ph]* (2016). URL <http://arxiv.org/abs/1609.00684>.
11. Kerviche, R., Guha, S. & Ashok, A. Fundamental limit of resolving two point sources limited by an arbitrary point spread function. *arXiv:1701.04913 [physics, physics:quant-ph]* (2017). URL <http://arxiv.org/abs/1701.04913>.
12. Yang, F., Nair, R., Tsang, M., Simon, C. & Lvovsky, A. I. Fisher information for far-field linear optical superresolution via homodyne or heterodyne detection in a higher-order local oscillator mode. *arXiv:1706.08633 [physics, physics:quant-ph]* (2017). URL <http://arxiv.org/abs/1706.08633>.
13. Tang, Z. S., Durak, K. & Ling, A. Fault-tolerant and finite-error localization for point emitters within the diffraction limit. *Opt. Express* **24**, 22004 (2016). URL <https://www.osapublishing.org/abstract.cfm?URI=oe-24-19-22004>. DOI 10.1364/OE.24.022004.
14. Yang, F., Tashchilina, A., Moiseev, E. S., Simon, C. & Lvovsky, A. I. Far-field linear optical superresolution via heterodyne detection in a higher-order local oscillator mode. *Opt.* **3**, 1148 (2016). URL <https://www.osapublishing.org/abstract.cfm?URI=optica-3-10-1148>. DOI 10.1364/OPTICA.3.001148.
15. Tham, W.-K., Ferretti, H. & Steinberg, A. M. Beating Rayleigh’s Curse by Imaging Using Phase Information. *Phys. Rev. Lett.* **118**, 070801 (2017). URL <http://link.aps.org/doi/10.1103/PhysRevLett.118.070801>. DOI 10.1103/PhysRevLett.118.070801.
16. Pařr, M., Stoklasa, B., Hradil, Z., Sánchez-Soto, L. L. & Rehacek, J. Achieving the ultimate optical resolution. *Opt.* **3**, 1144 (2016). URL <https://www.osapublishing.org/abstract.cfm?URI=optica-3-10-1144>. DOI 10.1364/OPTICA.3.001144.
17. Tsang, M. Subdiffraction incoherent optical imaging via spatial-mode demultiplexing. *New J. Phys.* **19**, 023054 (2017). URL <http://stacks.iop.org/1367-2630/19/i=2/a=023054>. DOI 10.1088/1367-2630/aa60ee.
18. Goodman, J. W. *Introduction to Fourier Optics* (McGraw-Hill, New York, 2004).
19. Goodman, J. W. *Statistical Optics* (Wiley, New York, 1985).
20. Miller, D. A. B. All linear optical devices are mode converters. *Opt. Express* **20**, 23985–23993 (2012). URL <https://www.osapublishing.org/abstract.cfm?uri=oe-20-21-23985>. DOI 10.1364/OE.20.023985.
21. Zmuidzinas, J. Cramér–Rao sensitivity limits for astronomical instruments: implications for interferometer design. *J. Opt. Soc. Am. A* **20**, 218–233 (2003). URL <http://josaa.osa.org/abstract.cfm?URI=josaa-20-2-218>. DOI 10.1364/JOSAA.20.000218.

22. Huber, M. C. E. *et al.* (eds.) *Observing Photons in Space: A Guide to Experimental Space Astronomy* (Springer, New York, 2013). URL [http://dx.doi.org/10.1007/978-1-4614-7804-1\\_16](http://dx.doi.org/10.1007/978-1-4614-7804-1_16).
23. Pawley, J. B. (ed.) *Handbook of Biological Confocal Microscopy* (Springer, New York, 2006).
24. Chao, J., Sally Ward, E. & Ober, R. J. Fisher information theory for parameter estimation in single molecule microscopy: tutorial. *J. Opt. Soc. Am. A* **33**, B36 (2016). URL <https://www.osapublishing.org/abstract.cfm?URI=josaa-33-7-B36>. DOI 10.1364/JOSAA.33.000B36.
25. Van Trees, H. L. *Detection, Estimation, and Modulation Theory, Part I*. (John Wiley & Sons, New York, 2001).
26. Deschout, H. *et al.* Precisely and accurately localizing single emitters in fluorescence microscopy. *Nat. Methods* **11**, 253–266 (2014). URL <http://dx.doi.org/10.1038/nmeth.2843>. DOI 10.1038/nmeth.2843.
27. Schützenberger, M. P. A generalization of the Fréchet-Cramér inequality to the case of Bayes estimation. *Bull. Amer. Math. Soc.* **63**, 142 (1957). URL <https://doi.org/10.1090/S0002-9904-1957-10102-5>. DOI 10.1090/S0002-9904-1957-10102-5.
28. Gill, R. D. & Levit, B. Y. Applications of the Van Trees inequality: A Bayesian Cramér-Rao bound. *Bernoulli* **1**, 59–79 (1995). URL <http://www.jstor.org/stable/3318681>.
29. Van Trees, H. L. & Bell, K. L. (eds.) *Bayesian Bounds for Parameter Estimation and Nonlinear Filtering/Tracking* (Wiley-IEEE, Piscataway, 2007).
30. NIST Digital Library of Mathematical Functions. <http://dlmf.nist.gov/>, Release 1.0.11 of 2016-06-08 (2016). URL <http://dlmf.nist.gov/>. Online companion to<sup>31</sup>.
31. Olver, F. W. J., Lozier, D. W., Boisvert, R. F. & Clark, C. W. (eds.) *NIST Handbook of Mathematical Functions* (Cambridge University Press, New York, NY, 2010). Print companion to<sup>30</sup>.
32. Arfken, G. B. & Weber, H. J. *Mathematical Methods for Physicists* (Elsevier, Amsterdam, 2005).

## Acknowledgments

This work is supported by the Singapore Ministry of Education Academic Research Fund Tier 1 Project R-263-000-C06-112.

## Additional Information

**Competing financial interests:** The author declares no competing financial interests.